Electromagnetic Design Improvements of the Single-Sided Disk-Rotor Induction Motor for the FST In-Wheel Traction

Nuno Miguel Macara, Instituto Superior Técnico

Abstract

With the increase in popularity of electrical vehicles and the need for more efficient machines, the optimization of electrical motors is of great importance. The aim of this thesis is to accurately characterize an axial induction machine, followed by the development of a finite element method model of the machine. This induction machine is intended to be an in-wheel motor for a vehicle. After the development of the model, several electromagnetic tests were performed, and the machine's geometry was optimized. The thermal behavior of the machine was also measured experimentally, and a thermal model of the machine was created. The results obtained show an improvement in the electromagnetic performance of the machine, despite its overall inefficiency for its purpose, with a much lower torque than needed. However, the FEM model proved to be very accurate for stationary simulations, and its application also very promising in different types of machine.

1. Introduction

1.1. Motivation

As society shifts into a more efficient and sustainable world, the need for electrical machines has never been greater, so new types of machines with different geometries have been created. These new machines tend to be smaller and more efficient, as electrical vehicles become more popular. The induction machine, due to its simplicity, is the most used type of electrical machine.

So, in 2017 student João Guilherme designed and modelled an axial flux induction machine for the formula student electric vehicle competition, Guilherme (2017). The motor's purpose was the propulsion of the electrical car, and intended to drive each wheel independently, using a total of 4 motors. This way, each motor can produce only 25% of the total power, and therefore can be smaller than one single large motor. As axial machines are shorter than "normal" ones, this type of design is ideal for this use, as the motors can be mounted inside the wheels.

With the competition rules and the desired performance specifications for the vehicle, table 1, it was calculated each motor nominal torque to be 208,35 Nm, for a 20 cm rotor diameter. Each motor would be powered by independent 3-phase 50 Hz sinusoidal currents, and all motors to be 1 pair of poles machines.

After the motor specifications created, both a mathematical and a physics simulation model were developed for the motor. The electromagnetic performance of the machine was analyzed, and then compared between both mathematical and simulation models. Due to the high complexity of the physics model, FEM, these simulations were only performed with a blocked rotor in the frequency domain. Figure 1 plots the comparison between both models, and both models show a very similar behavior. However, the results are far from the desired torque for the machine, 208,25 Nm. This difference mainly comes from the type of simulation, as the blocked rotor test produces no torque, as the name indicates, the rotor is blocked.

Maximum velocity	120 km/h
Maximum acceleration	9,26 m/s
Vehicle mass	300 kg

Table 1: Vehicle specifications.

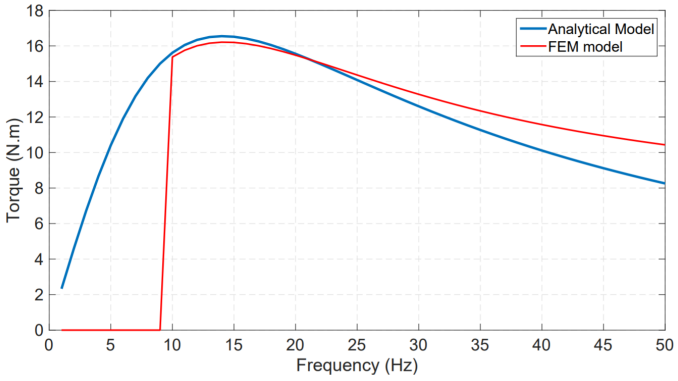

Figure 1: Torque/Frequency response with blocked rotor, for both analytical and FEM models.

Due to this, time-dependent tests were made, however the results also proved to be unsatisfying, with the final conclusion being the machine not working for its main purpose: the propulsion of the electrical vehicle. However, this motor could serve other applications, where the torque needed is lower. So, in 2019 student Francisco Fernandes built and tested the physical machine, Fernandes (2019) and fig. 2. The machine used the same geometry developed by Guilherme (2017), and a very promising new type of material, the Somaloy® soft composite metal alloy, Somaloy datasheet (2021).

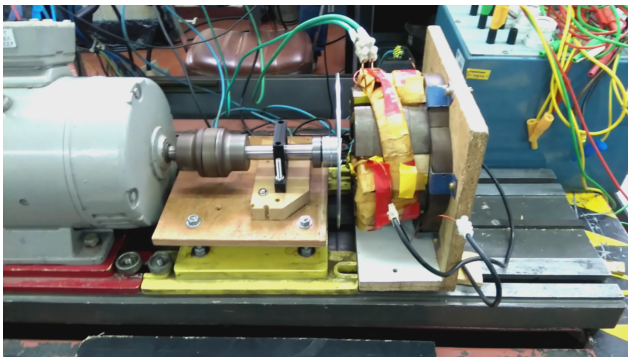

Figure 2: Axial induction motor test setup at IST's electrical machines' laboratory Fernandes (2019).

After the machine was built, it was tested in the electrical machines' laboratory at Instituto Superior Técnico in Lisbon, and the results showed the motor performance to be very low, much lower than the theoretical simulations. The source for this low performance is not trivial, since both models developed by Guilherme considered perfect materials and conditions, whereas in reality this does not occur. Due to this, a deeper analysis of this machine was necessary to better comprehend it.

1.2. Objectives

The aim of this work is to better characterize the axial induction motor, and to develop a new accurate finite element method model of the machine. The machine is analyzed through a series of electromagnetic experiments, and with the data a new 3D FEM model will be created. This model will allow through simulations more complex experiments, and consequently the acquisition of more complex. This data will then be used to optimize and further comprehend the full behavior of the machine. The thermal behavior of the machine will also be experimentally measured and a new thermal FEM model will be designed.

1.3. Document structure

This work can be structured into its Theoretical Background, where the physical principles of the machine are explained, and a linear analytical model of the machine is created and tested; the Stator Characterization, where the stator core of the machine is magnetically characterized, experimentally; the Finite Element Method Model, where a new 3D physical model is created and validated; the Simulation Results, where the most relevant outputs of the simulations are presented and commented; and the Conclusions and Future Work, where the major conclusions of the work are presented and what the possible outcomes of it.

2. Theoretical Background

2.1. Linear model

In the first work, Guilherme (2017), the induction motor was designed and modelled in a steady-state, and then it was built and tested in the Electrical Machines' Laboratory, Fernandes (2019). However, with several discrepancies in behavior, a new model is desirable So the first step for this model was creating a simple mathematical model. The first step was then converting the cylindrical machine to a linear one, a much simpler approach, with a more familiar orthogonal coordinate system, fig. 3 based on the work of Poitout (2005). This motor assumes a rectangular stator base, 6 rectangular teeth, and an also rectangular rotor.

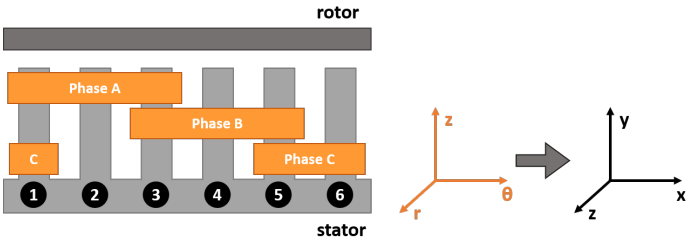

Figure 3: Equivalent linear motor and new coordinate system.

2.2. Analytical model

With a new, simpler, linear model, a bi-dimensional analytical model was developed, and the rotor force, responsible for generating the output power takes the form eqs. (1a) and (1b).

$$\mathbf{F} = \mathbf{J} \times \mathbf{B} \tag{1a}$$

$$\mathbf{F} = -J_z B_y \, \mathbf{u_x} \; + \; J_z B_x \, \mathbf{u_y}. \tag{1b}$$

The analytical model was then adapted to the machine's specifications, section 2.2. This linear model, however, is purely qualitative, as it only illustrated the basic functioning principles of the machine.

stator length	410 mm
stator height	100 mm
rotor length	410 mm
rotor thickness	15 mm
coil number of turns	60

Table 2: Linear motor dimensions.

3. Stator Characterization

3.1. Magnetization curve measurement motives

The motor's stator that is already constructed is made of a soft iron alloy, Somaloy ®, whose physical properties ended not matching the manufacturer's, as the previous works showed: the theoretical model developed in the first part was simulated with the product's specifications from the manufacturer, and the physical motor was built with the real material. However, as mentioned in 1.1, the experimental data did not match the simulated. Consequently, a more comprehensive electromagnetic characterization of the machine was needed.

3.2. Experiment

This characterization is done through the measurement of the magnetization curve of the stator core. This experiment uses a new 200 turn coil, and an auxiliary iron alloy disk, used to close the magnetic circuit between two consecutive stator teeth. This magnetization curve (BH) of the stator core was then measured with different voltages, the highest being 196 V. The final post-processed curve is presented in fig. 4.

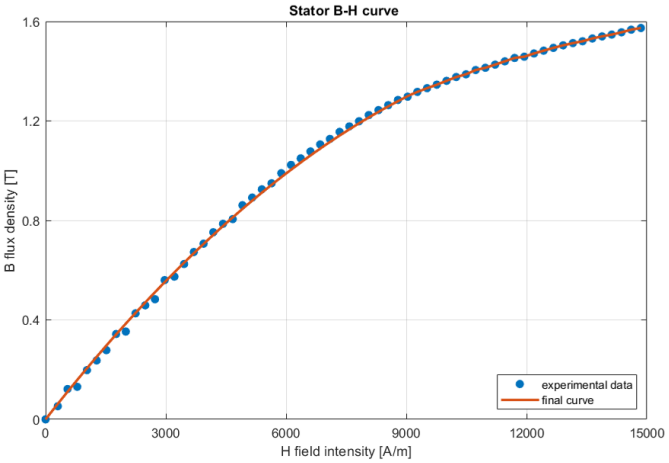

Figure 4: Experimental and fitted BH curves.

4. Finite Element Method Model

4.1. Geometry and Materials

To perform a more detailed and complete analysis of the machine, an equivalent 3D electromagnetic simulation model had to be developed. The Finite Element Method (FEM) was the used to solve the problem, with the use of a FEM simulation software. This model was designed with the actual dimensions of the real motor, and an additional sphere of air involving the main geometry, fig. 5. The model considers the real materials and their properties due to their significance, the most important being their conductivity and magnetic characteristics, section 4.1.

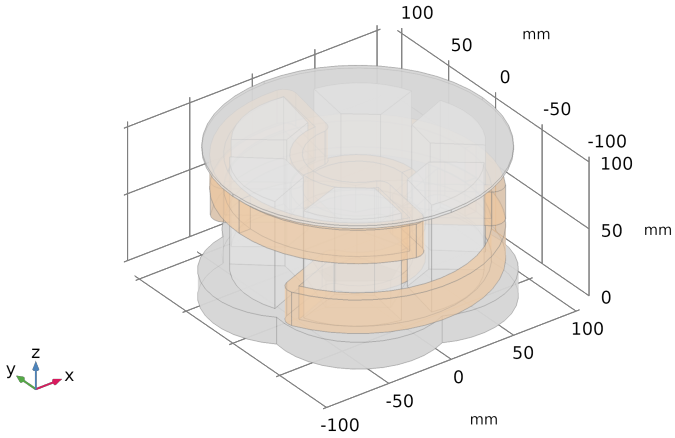

Figure 5: 3D render of the finite elements motor.

Material	electrical conductivity	BH relation
Stator iron alloy	5000 [S/m]	BH curve
Aluminum	$3.774 \cdot 10^7$ [S/m]	$\mu_r = 1$
Copper	$5.998 \cdot 10^7$ [S/m]	$\mu_r = 1$
Air	10 [S/m]	$\mu_r = 1$

Table 3: FEM model materials' electromagnetic properties

4.2. FEM electromagnetic Physics and Studies

The Physics step of the FEM model is the most important, since it sets the electromagnetic physics conditions and relations between the several components. There were a total of 2 different types of studies used: frequency domain and time domain. The most used, Frequency Domain (FD), considers all electromagnetic quantities sinusoidal, and was used in stationary steady-state conditions, where the rotor is blocked. The time domain was used less frequently, since it is much more computing heavy, and was only used in the Rotating Machinery Physics (RMM). This physics differs from the stationary with blocked rotor as it considers a rotational movement of the rotor.

4.3. FEM model validation

As previously tested, there are big discrepancies between the projected motor and the real constructed machine. So, after the modelling of the machine there is a need to validate the model and this way create a parallelism between both real and FEM models. Several experiments

were performed, and the FEM model adjusted accordingly.

After several experiments and simulations, the stator's core BH curve of the FEM model was adjusted accordingly, as to create an accurate bridge between the real and the simulated motor. This was done through the measurement of the stator's core BH curve, as in section 3.2. And then recreating the experiment with the FEM model. The coil's current and voltage were compared and a new modified FEM BH curve was created. This new BH relation, despite being different from the experimentally measured, replicates the physical results in the simulation. The new and "original" curves are depicted in fig. 6.

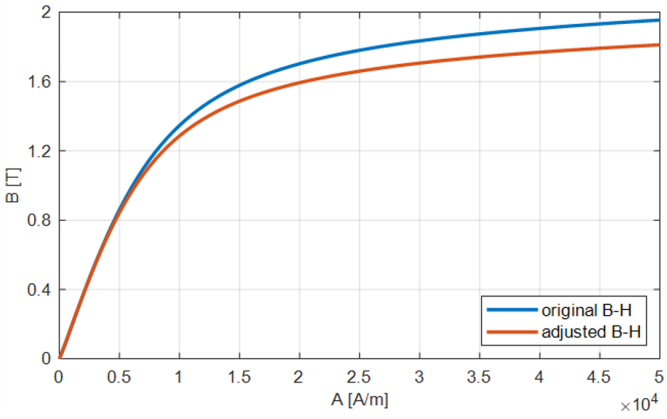

Figure 6: "Original" and adjusted BH curves.

5. Simulation Results

Having the FEM model validated, there is an equivalence between the simulation and the real motor. This parallelism is very important, as physical experiments are more expensive than simulated ones when it comes to experimenting new materials and different coil geometries, and also the existing limitations in the laboratory, like the available maximum voltage and temperature damage to materials, which in turn are easily overcome with the numerical model.

Several simulations were then run, most of them with a blocked rotor, for the electromagnetic study of the machine, with an emphasis on the stator study, as the behavior of the magnetic field there created will dictate the functioning of the machine. As said, most simulations were performed with a frequency domain study, as the motor is designed to function within its materials' normal operating conditions, i.e. within the linear zone of their BH curves and therefore all quantities will remain sinusoidal.

After the first set of frequency domain studies, some experiments were performed with the rotating machinery physics and solved time dependent studies. However, due to some inconsistencies in the stator's magnetic penetration, these results can only be appreciated as qualitative, not quantitative. At last, the final simulations were again frequency domain studies, however now with several modifications to the machine's coils and rotor. The rotor modifications regard its thickness, and the coils modifications regard its geometry, pair of poles and number of turns.

5.1. Motor analysis

5.1.1. Stator and coil analysis

The first important results regard the stator and the coils of the machine, since they generate the magnetic flux responsible for the rotor induced currents and consequently, the torque of the machine. With a phase voltage of 20 V, 50 Hz, the coil's current density is plotted for the blocked rotor frequency domain study in fig. 7.

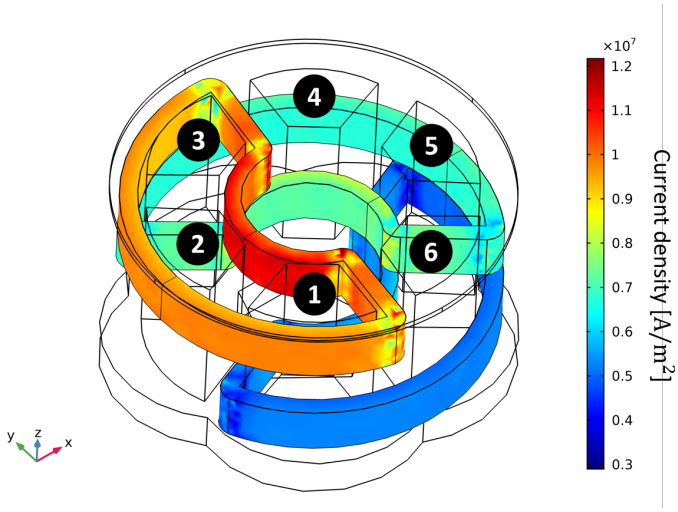

Figure 7: Coils current density distribution for 3-phase 20V excitation.

This shows different current density values in all coils, which will cause a very different magnetic flux distribution in the stator core. Figure 8 plots the vertical flux density distribution in the stator's top surface for the same conditions as fig. 7.

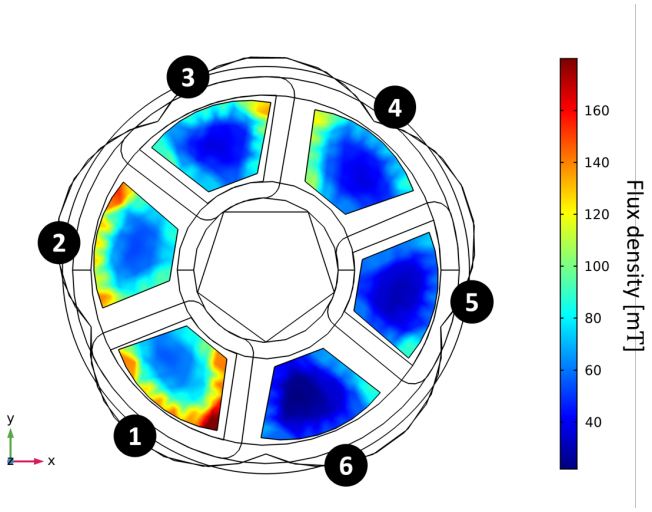

Figure 8: Stator top surface magnetic flux density z-component.

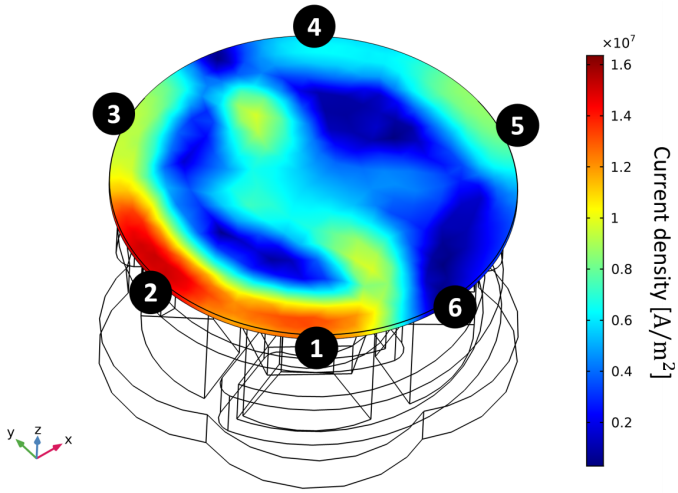

Figure 9: Rotor induced current density norm for the x and y-components.

From fig. 8 one can immediately see how poor the flux density distribution in the stator's top surface is. With values ranging from 60 to 170 mT in tooth 1, to ranging from 0 to 90 mT in tooth 5. Not only these values are very low, but also they demonstrate a very uneven flux distribution.

After the stator and coil analysis, most of the machine's flaws are already identified: firstly, the air-gap flux generated at the stator, responsible for generating the rotor's induced currents and the magnetic flux density, was proven to be very small. Usually, the flux density is between 1 and 2 T for a similar size machine (10/20 times higher the measured values), so the rotor induced currents will in turn be small as well.

5.1.2. Rotor analysis

Figure 9 represents the norm of the induced current density in the x and y-axis. The z-axis component is neglected as the rotor's developed torque is a result of the cross product between the vertical flux, B_z, and the rotor's induced current density plane normal to it, J_x and J_y.

The current density in the rotor is induced by the vertical flux density in the air gap above the teeth top surface and, as we can observe infig. 9, it is highly concentrated around the edges of the rotor, right above the teeth. This is a direct result of the flux density being much higher in the teeth edges, as shown in fig. 8. As expected, there is a big disparity in the values in the figure, an 8 times difference above teeth 2 and 6, as a result of the coils' positioning. Due to this uneven J distribution, the machine is very unbalanced, which will create forces in the rotor that are not axial, and consequently create vibrations on the rotor, which have already been observed in the laboratory in the previous works.

The rotor developed force is then a consequence of the interaction between the stator's generated flux density and the rotor's current density. However, with values so small it is expected the starting torque and the Lorentz force to be small as well. Section 5.1.2 shows the calculated axial starting torque and the 3 components of the Lorentz force. fig. 10 shows the rotor developed force vector.

axial Torque	Force x	Force y	Force z
0.16 Nm	2.01 N	1.33 N	15.78 N

Table 4: Rotor developed forces: axial, and Lorentz x, y and z-components.

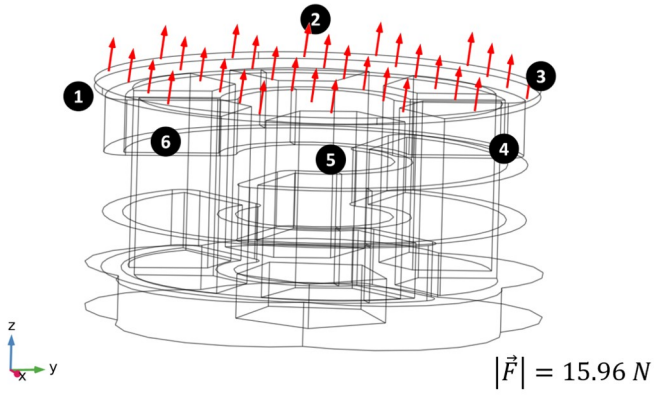

Figure 10: Rotor developed force vector.

The axial torque, responsible for the rotation of the machine, is a combination of both x and y-axis components of the force, and the z-component is responsible for the vertical movement of the motor, in this case positive. This translates to a force pushing the rotor away from the stator, in this case a force practically 10 times higher in the vertical direction, quite visible in fig. 10, unwanted,

than in the horizontal plan, wanted. This upward is a result of the induced currents that create an opposing magnetic field, which creates a repulsion between them.

The starting torque, normally smaller than the nominal torque, is in this case much smaller than originally designed. This is a direct result of the very low values of flux and current densities. However, due to being a starting torque at 50 Hz one cannot extrapolate the full behavior of the machine, so additional studies were performed.

5.2. Frequency Domain - [5-60] Hz

As a variation of frequency causes a variation in the coil generated magnetic flux, some additional simulations were done varying the electrical frequency of the motor input. The vertical flux density at the stator's top surface and the starting torque of the machine are plotted in figs. 11 and 12, respectively. Frequencies vary between 5 and 60 Hz, and as expected, with a higher frequency the torque is smaller. However, as mechanical power is proportional to the rotor velocity, and consequently the electrical frequency, one cannot extrapolate the power output of the machine.

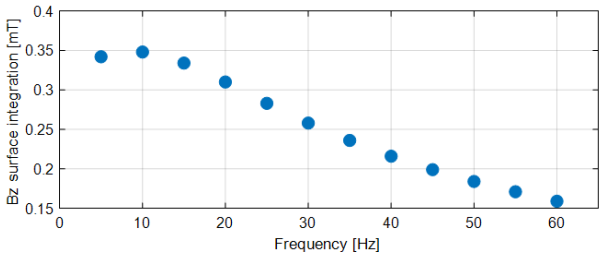

Figure 11: Stator top surface total $\mathbf{B}_z$ for [5;60] Hz.

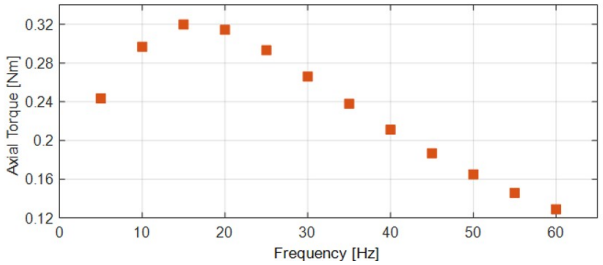

Figure 12: Rotor starting torque for [5;60] Hz.

5.3. Rotating Machinery

5.3.1. Rotating Machinery vs Frequency Domain

Due to the limitations of the frequency domain blocked rotor studies used, a rotating machinery study would be ideal, since it considers the velocity of the rotor and the interactions unique to this movement. However, when both FD and RMM results are compared, figs. 13 and 14 respectively, there is a discrepancy between the vertical flux distribution.

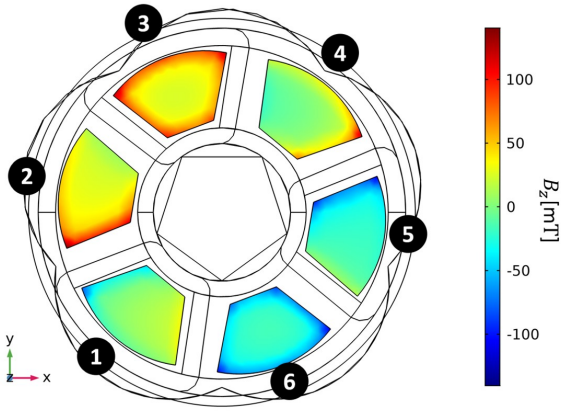

Figure 13: Rotating machinery top surface flux density z-axis.

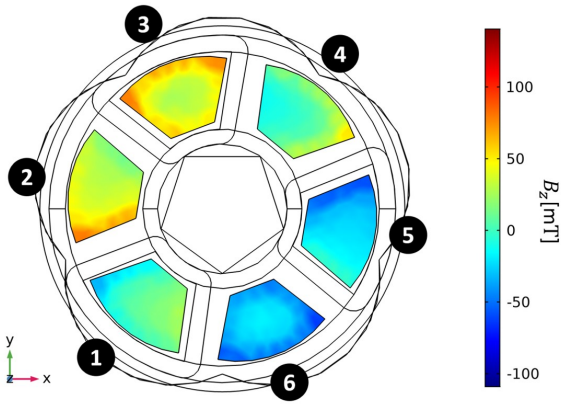

Figure 14: Frequency domain top surface flux density z-axis.

In the RMM, fig. 13, the flux does not penetrate the stator teeth as much as in the FD, fig. 14, a result of the conditions set in the physics of the model. These conditions are necessary since they lower the complexity of the model. Without them the available computing power cannot solve the model. However, since the flux values from the RMM simulations are not correct, this model can only be seen as qualitative, again.

5.3.2. Rotating Machinery: 2900 RPM

Despite having an understanding of the magnetic flux distribution at the stator's top surface in the frequency domain, the time domain behavior is unknown. So, with the new qualitative RMM model, a new 50 Hz simulation was done, similar to before, however now at a rotor speed of 2900 RPM, instead of 0 (blocked rotor). The average $\mathbf{B}_z$ per tooth is plotted for 1 cycle, 20 ms, in fig. 15.

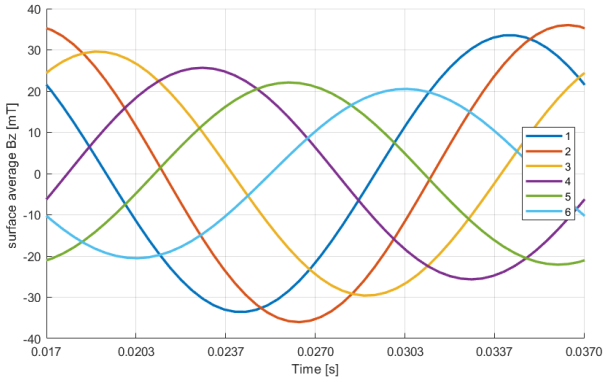

Figure 15: Average $\mathbf{B}_z$ per tooth for one 50Hz cycle.

From fig. 15 the full behavior of the flux density can be seen: each tooth flux, despite sinusoidal, has a different amplitude and mean value, so the resulting travelling magnetic wave in the air-gap not only is non-sinusoidal, it will be unbalanced. This is visible in fig. 16, where this resulting wave is plotted at t=0 and t=P/2, at the beginning and at the middle of the cycle. The dashed lines represent a sinusoidal wave with the same amplitude as the highest resulting wave. From the comparison of both waves one concludes how unbalanced the machine is.

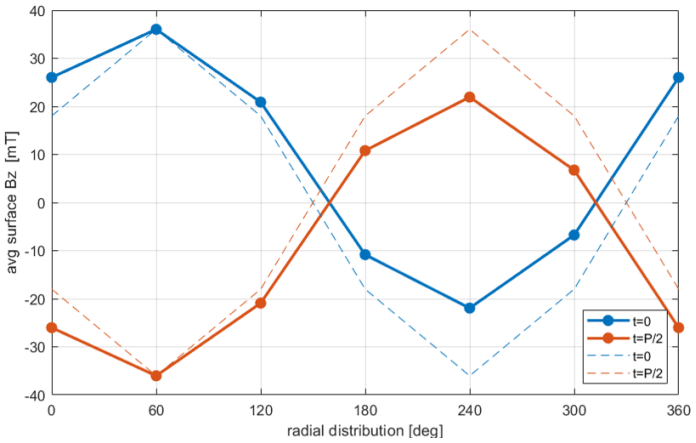

Figure 16: Resulting travelling magnetic field radial distribution, for t=0 and t=P/2.

5.4. Improvements

5.4.1. Stator

After the analysis of the machine, both with FD and RMM studies, some improvements on the motor were tested. The first improvements regard the stator's core material. Several materials were compared here, the current soft composite, electrical steel and laminated electrical steel. This layered material combines the properties of a low conductivity material and a highly permeable material. Section 5.4.1 shows the computed torque and levitating force on the rotor for the 3 materials. Comparing now the axial torque of all options, the highest is with the current material. With this current geometry, there is no need to build a new stator core.

material	z-Force	axial Torque
Somaloy	5.6 N	0.099 Nm
electrical steel	3.23	0.022 Nm
laminated electrical steel	5.34	0.073 Nm

Table 5: Stator core materials' properties.

5.4.2. Stator coils

With the stator unmodified, the next most important elements of the machine are the coils. As seen in fig. 8 there is a great unbalance due to the coil's vertical distribution, so new coils were designed. The new design considered a set of 6 concentrated coils, each wound around a stator tooth, fig. 17. These coils allow a much higher number of turns, a nearly perfect radial symmetry, and are closer to the air-gap, causing less leakage. Figure 18 plots $|\mathbf{B}_z|$ for the new coil set, and immediately one sees the exact same flux distribution at the stator. Completely different from fig. 8, where every tooth shows a different distribution. However small the highest flux density values are for the new coils, this simulation used the same number of turns of 60. The available space, however, allows for a total number of 150 turns, 2.5 times the current. As the axial torque is proportional to the number of turns, this would cause a 250% increase in the power output.

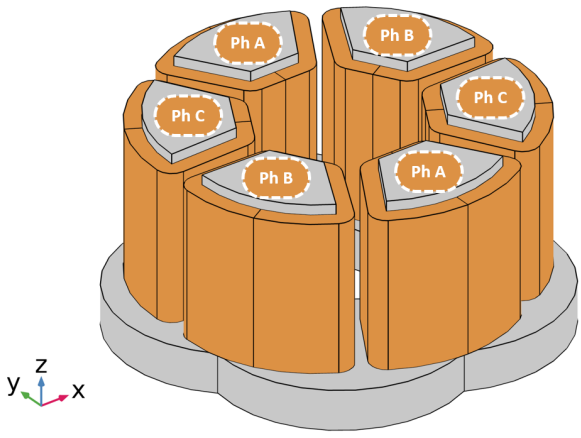

Figure 17: Stator with new concentrated coils.

5.4.3. Rotor

The rotor modifications made regard the material, much like the ones in the stator. Here different materials were compared, with also different conductivities and permeabilities. The rotor thickness was also varied between 3 and 20 mm, with both coil typologies. As expected, the

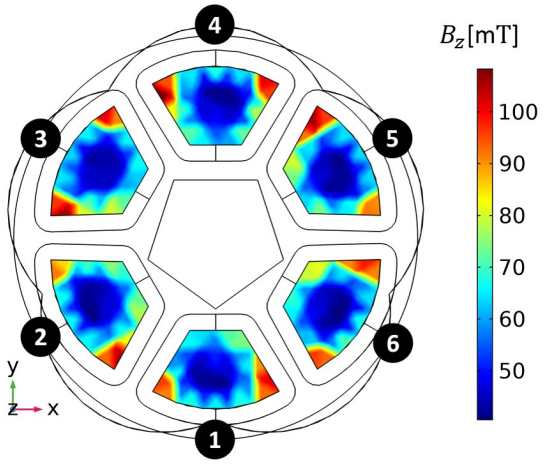

Figure 18: $|\mathbf{B}_z|$ top view for new coils.

increase in thickness of the rotor causes an increase in the induced current density, fig. 19. However, the increase in current density also causes an increase in the reactive opposing flux, lowering the total flux density.

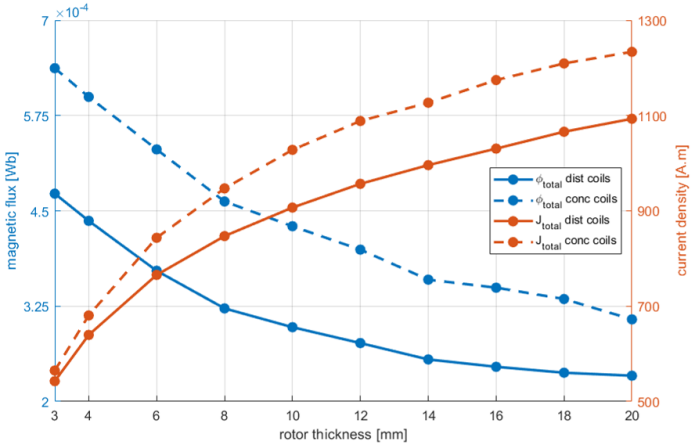

Figure 19: Total magnetic flux and rotor current density for both coil typologies, rotor 3-20 mm, 50 Hz.

When varying the materials properties, the conductivity of the rotor does not have a great impact on the torque, however an increase in the magnetic permeability has. In table 6 the vertical force and the axial torques are computed for each type of material. From this one concludes a higher permeability material would be better, $\mu_r \geq$1500, with a conductivity around 5000 S/m.

5.5. *Thermal model*

This machine efficiency, as already proven, is very low when compared to "normal" induction machines, i.e. axial rotor machines, whose efficiency can be higher than 90%. As thermal losses are a big part of any electromechanical device, its analysis is of great importance. To analyze the thermal behavior of this machine, the rotor Joule losses were measured eq. (2), first in the laboratory and then with a FEM thermal study,

σ [S/m]	μ_r	z-Force [N]	axial Torque [N*m]
0.1	1	4.011	$3.93{\cdot}10^{-3}$
	1500	-299.71	$84.99{\cdot}10^{-3}$
	3000	-324.35	$97.58{\cdot}10^{-3}$
	4500	-333.44	$102.29{\cdot}10^{-3}$
$5{\cdot}10^{3}$	1	4.0106	$3.95{\cdot}10^{-3}$
	1500	-299.71	$87.37{\cdot}10^{-3}$
	3000	-324.36	$100.25{\cdot}10^{-3}$
	4500	-333.44	$105.07{\cdot}10^{-3}$
$3.7{\cdot}10^{7}$	1	5.636	$92.18{\cdot}10^{-3}$
	1500	-22.126	$103.51{\cdot}10^{-3}$
	3000	-22.238	$102.81{\cdot}10^{-3}$
	4500	-22.273	$102.56{\cdot}10^{-3}$

Table 6: Rotor vertical force and axial torque for different rotor's properties with concentrated 60 turns coils.

$$P_{Joule} = J \cdot E = \frac{J^2_{ind\,rotor}}{\sigma_{Al}} \tag{2}$$

5.5.1. *Thermal experiment*

The laboratory experiment used a set of thermal probes and the machine was powered a phase RMS voltage of 16.2 V, phase RMS currents of 15.25, 13.16 and 12.62 A. The test duration was 31 minutes. Figure 20 plots the rotor and top coil temperature evolution during this time.

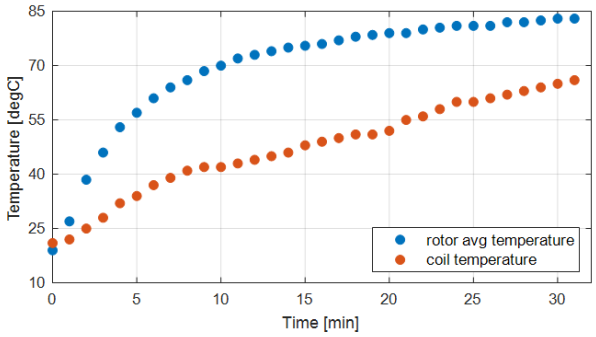

Figure 20: Top coil and rotor average temperature evolution.

The rotor's maximum achieved temperature is approximately 85 C for these currents, as it reaches saturation by the end of the experiment. However, as the rotor losses are a result of the induced current density, they are proportional to the input power: the higher the input power, the higher the losses and temperature.

5.5.2. *Thermal FEM model*

Now a finite elements' simulation is developed to compare the thermal behavior in the rotor. This model considers the rotor as a heat source with a heat rate equal to the power electrical power losses, P_{rotor}=43 W. With an initial temperature of 18 C, the same as the laboratory experiment. Figure 21 plots the final surface temperature of the motor

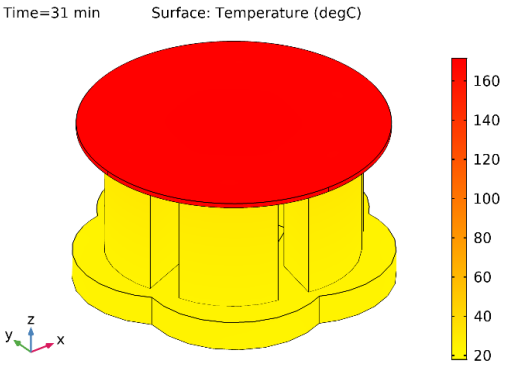

Figure 21: Motor surface temperature at t=31 minutes.

From fig. 21 it is visible the disparity of values in comparison with the real final temperature of 84 C. The source of this disparity is connected to the geometry itself, as the rotor is considered to be floating above the stator, with no physical connections; therefore, all the heat is used to increase its temperature and the stator's. However, the final temperature on the stator surface is of 34 C, much lower than the rotor's, above 160 C. This means most of the energy is used to solely increase the rotor's temperature, thus a more accurate model is needed. This new model, fig. 22 considers both coupling pieces **(1,4)**, the bearings **(2,3)**, and the axle **(5)**, all with equivalent mass and volume as the real components.

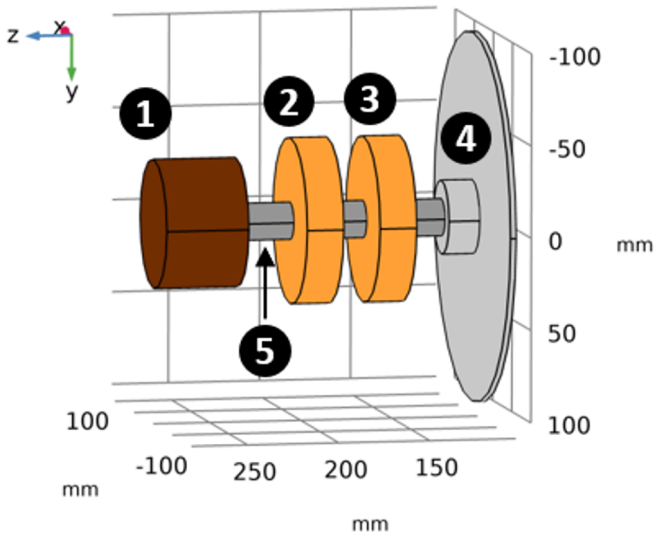

Figure 22: Complete FEM axle.

The final simulation was then run with the new axle and power, and the rotor's average surface temperature was plotted for the same time steps as the experimental. Figure 23 compares both experimental and simulated rotor's temperatures.

From the 2 datasets one can observe that despite having very similar final temperatures, the curve aspect is different, as the experimental temperature at the rotor surface practically achieved saturation by the end of the experiment, which is another reason for the duration of it, and the simulated one did not. This is a result of the assumptions made to create the thermal model, and of non-ideal testing equipment, since the FEM model measurements result from an average of 408 surface points, and the lab measurements use an average of 3.

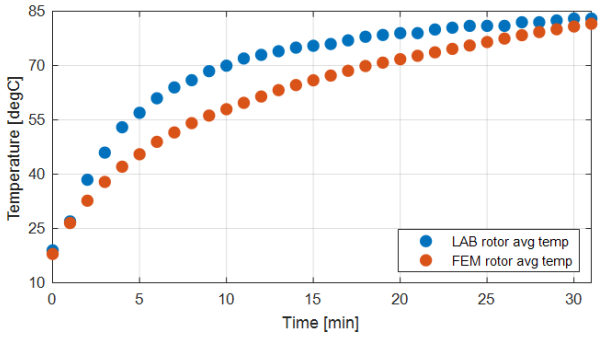

Figure 23: Experimental and simulated rotor temperature evolution.

6. Conclusions and Future Work

6.1. Conclusions

The stator core of the induction machine, the most relevant component of this motor was characterized, both experimental and simulation wise. This allowed a more accurate modeling and understanding of the magnetic behavior of the soft core material.

With this characterization a new FEM model was created, much more accurate than before. This model considered the real materials and properties of the machine. After it, the modelled was validated, new types of studies were developed and compared, and new simulations were run. The machine's electromagnetic properties were mapped and its behavior understood. The full functioning principles of the machine were learned and its flaws discovered. This led to new simulations where the machine's main components, its stator, stator coils and rotor, were modified. These modifications took advantage of the existing components, optimized them, and ultimately improved its overall functioning and efficiency. The final form of the machine considered the initial stator core of the machine, as no modifications proved a significant improvement; the stator coils were completely redesigned, and the new set of 6 coils performs much better than the original; the rotor geometry needed no modifications, however a new material would bring some improvements.

Due to the global pandemic no more laboratory work was possible, and none of the improvements on the machine could be tested.

The final model of the machine regarded its thermal behavior. The machine was tested in the laboratory and with this data a thermal model was created. The model was then adjusted and finally compared with the physical behavior. Ultimately the thermal model did not prove itself very accurate due to its complexity.

6.2. Future Work

Having now an accurate simulation model of the electrical machine and a new optimized design created, several routes for future work are created.

The first route considers the construction of the new set of coils on the current motor and the testing of the same. This would further validate the FEM model and some additional improvements could arise from this work, and ultimately, a better, more efficient machine.

The other route regards solely the electromagnetic simulations. The work until here developed could serve as a blueprint to the 3D simulation of different machines. Not only the existing models could be optimized, and with a higher computing capacity new, more complex and realistic models could be developed.

References

Fernandes, F. A. C. (2019). Design optimization of a single-sided disk-rotor induction motor for the fst in-wheel traction. Master's thesis, Instituto Superior Técnico.

Guilherme, J. D. T. (2017). Electromagnetic design of a single-sided disk-rotor induction motor for electric propulsion. Master's thesis, Instituto Superior Técnico.

Poitout, S. A. (2005). Modelização de um sistema de trasnporte de fluidos por forças electromagnéticas. Master's thesis, Instituto Superior Técnico.

Somaloy datasheet (2021). Somaloy 3p material datasheet. https://www.hoganas.com/globalassets/download-media/sharepoint/brochures-and-datasheets—all-documents/somaloy-3p$_m aterial - data_j une_2018_2273 hog.pdf$.